Check for updates

Thermodynamic and mechanical properties of supramolecular gel based on bisterpyridine ligand formed *via* a cooperative model

Yumi Park,[a] Minju Nam[a] and Jong Hwa Jung [ORCID] *[ab]

Supramolecular gels hold immense potential in materials science, particularly in the development of functional materials for optoelectronics, sensors, and soft robotics. Their tunable mechanical properties and hierarchical self-assembly facilitate precise control over material structures and functions. Herein, we present a comprehensive study of the photophysical and mechanical properties of a supramolecular gel derived from a bisterpyridine ligand. The bisterpyridine ligand **1**, incorporating alanine moieties as chiral units, was successfully synthesized. Notably, **1** exhibited gelation in aromatic solvents such as toluene and xylene, forming a supramolecular gel with a distinctive twisted fiber morphology. The heating and cooling curves exhibited non-sigmoidal shapes, indicating that supramolecular gel **1** prepared in toluene, was formed *via* a cooperative mechanism. The Gibbs free energy was calculated to be -32.82 kcal mol^{-1}. Furthermore, supramolecular gel **1** displayed strong blue emission, highlighting its potential for optoelectronic applications. The mechanical properties of **1** were investigated *via* rheometry, revealing a pronounced thixotropic behavior, indicative of a reversible gelation process. These findings underscore the adaptability and multifunctionality of supramolecular gel **1**, making it a promising candidate for advanced material applications.

Introduction

Supramolecular gels have emerged as a significant class of soft materials due to their unique self-assembly behavior, tunable mechanical properties, and stimuli-responsive characteristics.[1–16] Unlike conventional polymeric gels, which rely on covalent cross-linking, supramolecular gels are formed through non-covalent interactions such as hydrogen bonding, π–π stacking, metal coordination, and van der Waals forces.[7,17–20] This dynamic and reversible nature of supramolecular interactions allows these gels to exhibit self-healing, adaptability, and reconfigurability, making them highly attractive for various applications.[17,21–27] In addition, supramolecular gels form soft solids with high viscosity and viscoelasticity.[28–30] Their structural integrity is maintained by an entangled and partially branched fibrous network, which immobilizes the solvent phase and enables sol–gel transitions in response to external stimuli such as temperature, pH, and ionic strength.[17,18,31–34] In contrast, the supramolecular polymers described in our previous studies exist as homogeneously dispersed solutions lacking a percolated network structure, resulting in extremely low viscoelasticity.[35–37]

Terpyridine (TPY) ligands are renowned for their strong chelating ability with transition metals, facilitating the formation of supramolecular assemblies.[3,5,6,38,39] Their distinctive electronic and structural properties make them exceptional candidates for gelator design. Supramolecular gels formed by terpyridine ligands exhibit dynamic and reversible characteristics, enabling them to respond to environmental changes such as temperature, pH, and solvent polarity. Due to these attributes, terpyridine-based gelators have found applications in catalysis, optoelectronics, and biomedical engineering. Terpyridine ligands exhibit robust coordination complexes with transition metals such as Pt(II), Pd(II), Zn(II), and Fe(II), leading to the formation of extended networks and gel structures. The coordination process enhances the stability of the gel, providing unique mechanical and optical properties. Metal–organic gels based on terpyridine coordination can be designed to exhibit selective ion-responsive behavior, making them highly suitable for targeted applications.[2,22,38,40–42] The aromatic terpyridine core promotes π–π stacking interactions, facilitating supramolecular aggregation and gelation. Additionally, hydrogen bonding between functional groups within the gelator molecules further stabilizes the gel matrix. These non-covalent interactions enable the formation of reversible and stimuli-responsive gels with tunable properties.

Terpyridine-based gels serve as highly efficient catalytic platforms, particularly in oxidation–reduction reactions.[4,40,41,43,44] The synergy between metal coordination and

[a]Department of Chemistry, Gyeongsang National University (GNU), Jinju 52828, Republic of Korea. E-mail: jonghwa@gnu.ac.kr

[b]Research Institute of Advanced Chemistry, Gyeongsang National University (GNU), Jinju 52828, Republic of Korea

supramolecular network formation enhances the catalytic activity and recyclability of these systems. Hybrid nanocatalysts embedded within terpyridine gels represent a promising approach for both homogeneous and heterogeneous catalysis. The unique electronic properties of terpyridine-metal complexes enable their application in optoelectronic devices, including organic semiconductors and photodetectors.[2,45] Furthermore, terpyridine-based gelators have been employed as colorimetric and electrochemical sensors for metal ion detection.[46–49] Their ability to modulate optical properties in response to external stimuli makes them ideal candidates for smart sensor development. Biocompatible terpyridine-based gels are increasingly being investigated for drug delivery and tissue engineering applications.[49–51] The reversible nature of their self-assembly allows for controlled drug release, responding to changes in pH, temperature, or ionic strength. Additionally, these materials have demonstrated potential in biosensing applications, including DNA and protein detection.[49,52–55]

Terpyridine-based gelators represent a promising class of supramolecular materials with extensive applications in catalysis, optoelectronics, and biomedicine. Understanding their gelation mechanisms and optimizing their self-assembly properties will facilitate the development of next-generation functional materials. Future research should focus on enhancing the stability and responsiveness of terpyridine gels while exploring their integration into advanced material systems. Continued advancements in this field are expected to yield innovative solutions for diverse technological and scientific challenges.

Hence, integrating amide units with terpyridine groups in molecular design, using straightforward synthetic methods, are a critical strategy for developing supramolecular gels both in the presence and absence transition metal ions. Compound **1** is designed with two terpyridine moieties that impart hydrophobic character and facilitate π–π interactions, alongside two chiral alanine units that introduce hydrophilicity and enable intermolecular hydrogen bonding during gel formation. Owing to this balanced amphiphilic architecture, compound **1** is anticipated to exhibit both hydrophobic and hydrophilic properties, thereby promoting the formation of supramolecular gels in organic solvents. Here, we report on the gelation behavior of bis(terpyridine)-based ligand **1** containing two *R*-alanine units in toluene and xylene (Fig. 1). The photophysical and mechanical properties were investigated using UV-Vis, photoluminescence spectroscop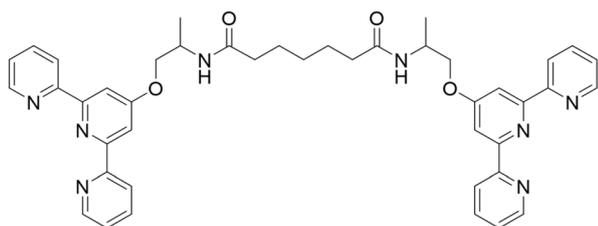y and rheometry. In addition, the thermodynamic parameters of supramolecular gel **1** were calculated based on heating and cooling experiments.

Results and discussion

Compound **1**, featuring two terpyridine and alanine moieties, was synthesized as illustrated in Scheme S1 and thoroughly characterized by ^{1}H and ^{13}C NMR spectroscopy, FT-IR, and ESI-MS (see SI: Fig. S6–S11). Comprehensive characterization data are provided in the SI.

We first investigated the gelation behavior of compound **1** in various organic solvents. It was found that **1** could form gels in organic solvents such as toluene and xylene (Fig. 2) including ACN, DCM, DMF, DMSO, chloroform, methanol and 2-propanol (Fig. S1 and Table S1). These findings suggest that **1** can serve as a building block for organogel formation. The critical gelation concentrations (CGC) of compound **1** in toluene and xylene were determined to be 0.7 and 0.5 wt%, respectively (Fig. S2).

Notably, the gelation behavior of **1** differs significantly from that of the supramolecular polymer previously reported in our study, which was formed in a mixed DMSO and H_2O (3 : 7 v/v) system.[56] This distinction arises despite both systems relying on intermolecular interactions such as hydrogen bonding, π–π stacking, and van der Waals forces for self-assembly. The underlying driving forces governing gel formation will be discussed in detail later.

To investigate the morphology of the synthesized supramolecular gel, we acquired scanning electron microscopy (SEM) and atomic force microscopy (AFM) images of supramolecular gel **1** formed in toluene. The SEM and AFM images revealed the formation of twisted fibers with lengths extending to several hundred micrometers (Fig. 3). Notably, these fibers exhibited extensive entanglement, which likely facilitated gelation by encapsulating solvent molecules. In contrast, such pronounced fiber entanglement was rarely observed in supramolecular polymers formed in dilute solutions. This extensive fiber entanglement is presumed to play a crucial role in the gelation process.

The UV-Vis and photoluminescence (PL) spectra of organogel **1** and monomer **1** were recorded at two different solvents (Fig. S3). The UV-Vis absorption band of supramolecular gel **1** was observed at 300 nm, corresponding to the π–π* transition of the bisterpyridine moiety. In contrast, the absorption band of monomer **1** in CH_2Cl_2 appeared at 275 nm. The red-shifted absorption of supramolecular gel **1** suggests the formation of

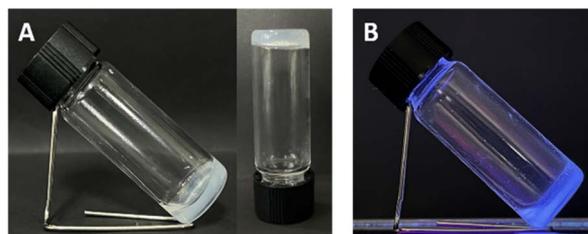**Fig. 1** Chemical structure of compound **1** in this study.

Fig. 2 Photographs of **1** supramolecular gel in toluene under (A) ambient light and (B) UV light.
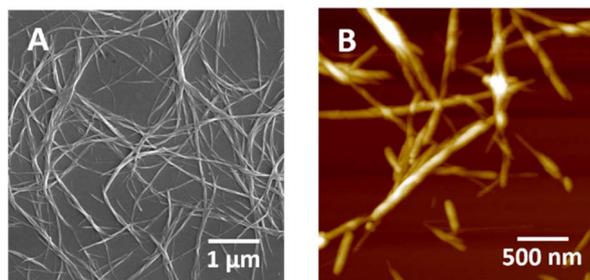
Fig. 3 (A) SEM and (B) AFM images of supramolecular gel **1** (1 wt%) formed in toluene.

a supramolecular gel stabilized by $\pi-\pi$ stacking interactions between the bisterpyridine units. Furthermore, the PL spectrum of supramolecular gel **1** exhibited a red shift compared to that of the monomeric species in CH_2Cl_2, further indicating the influence of supramolecular assembly on its photophysical properties.

Temperature-dependent UV-Vis spectral changes of supramolecular gel **1** were monitored at 350 nm (Fig. 4). No significant changes in absorbance at 350 nm were observed between 293 K and 313 K. However, at 318 K, the absorbance at 350 nm dramatically decreased, indicating the dissociation of the supramolecular gel into monomeric species. These results demonstrate that supramolecular gel **1** remains stable at temperatures below approximately 316 K. In particular, the heating and cooling curves exhibited non-sigmoidal shapes, indicating that the supramolecular gel forms *via* a cooperative mechanism involving nucleation and elongation. Furthermore, the thermodynamic parameters of supramolecular gel **1** were evaluated using a cooperative model (Table S2). The Gibbs free energy derived from the heating curve was calculated to be -32.82 kcal mol^{-1}. Quantitative analysis also yielded a cooperativity parameter, σ defined as the ratio of the nucleation constant (K_n) to the elongation constant (K_e)—ranging from 2.3×10^{-3} to 5.2×10^{-4}, based on curve fitting with the cooperative model.
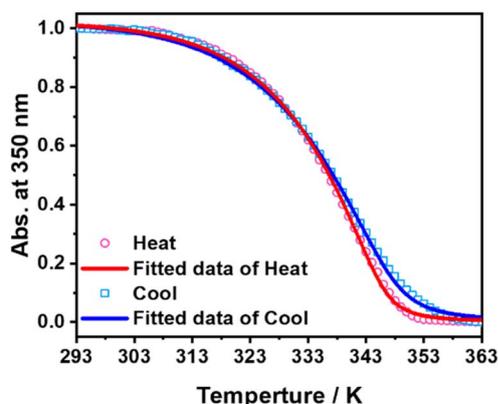

Fig. 4 Plots of temperature-dependent changes in the degree of aggregation (monitored at 350 nm) for supramolecular gel **1** (0.7 wt%) in toluene, recorded at a heating rate of 1.0 K min^{-1}. To obtain an accurate T_e, the heating curve was measured at 0.7 wt%.

To elucidate the driving forces behind gel formation, we obtained the ^1H nuclear magnetic resonance (NMR) spectrum of **1** (1 wt%) in toluene-d_8. At 298 K, the aromatic proton signals (H1, H2, and H3) of **1** appeared significantly broadened (Fig. S4a), indicating the presence of strong $\pi-\pi$ stacking interactions between the bisterpyridine units (Fig. S4). In contrast, at 353 K, the aromatic proton peaks became sharper and exhibited a downfield shift compared to those at 298 K (Fig. S4a and c), suggesting the dissociation of the supramolecular nanoarchitecture into monomeric species. Additionally, in CDCl$_3$, the aromatic proton peaks were sharper and displayed a downfield shift (Fig. S4d), indicating the presence of weaker $\pi-\pi$ stacking interactions at 298 K in toluene-d_8. We conducted Fourier-transform infrared (FT-IR) spectroscopy to further investigate its supramolecular interactions. The amide I band of supramolecular gel **1** appeared at 1635 cm^{-1} (Fig. S5a, right panel). In contrast, in CH$_2$Cl$_2$, the amide I band was observed at 1670 cm^{-1} (Fig. S5b, right panel). The –NH stretching band of supramolecular gel **1** appeared at 3286 cm^{-1}, whereas the –NH stretching band of monomer **1** in CH$_2$Cl$_2$ was observed at 3694 cm^{-1}. These results imply that the –NH moieties in supramolecular gel **1** participate in intermolecular hydrogen bonding interactions. These results strongly suggest that supramolecular gel **1** forms a supramolecular nanoarchitecture through robust intermolecular hydrogen bonding between the amide groups.[57-59] further stabilizing the gel network.

The mechanical properties of supramolecular gel **1** were investigated using rheometry. The storage modulus (G′) and loss modulus (G″) were plotted as a function of strain to provide insights into the viscoelastic nature of supramolecular gel **1** (Fig. 5A). At low strain levels (0.1–10%), the storage modulus (G′) is significantly higher than the loss modulus (G″), indicating that the material primarily exhibits elastic behavior. This suggests the presence of a well-entangled, structured network, characteristic of supramolecular gels or physically crosslinked polymer systems. In this regime, the material maintains its structural integrity under small deformations. As strain increases (10–100%), both G′ and G″ gradually decrease, reflecting a weakening of the network structure. This reduction in moduli suggests that the material is undergoing molecular rearrangements and softening while still retaining partial elasticity. This intermediate strain region indicates that the network is not yet permanently disrupted, though supramolecular interactions begin to yield under increasing deformation. At higher strain levels (>10%), G′ and G″ continue to decrease, and a critical crossover point is observed where G″ surpasses G′. This transition signifies a shift from a solid-like (elastic) state to a liquid-like (viscous) state, marking the onset of yielding. Beyond this point, the structural integrity of supramolecular gel **1** is lost, and the material flows under applied deformation, demonstrating the breakdown of the entangled fiber network.

Fig. 5B presents the frequency-dependent oscillatory rheological behavior of the supramolecular gel, illustrating the G′ and the G″ as functions of angular frequency (ω). Across the entire frequency range examined, G′ remains significantly higher than G″, with both moduli exhibiting minimal
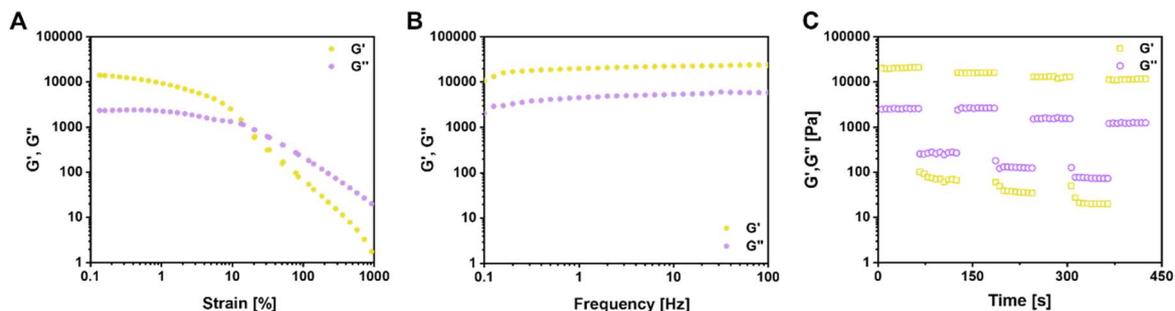
Fig. 5 Rheological properties of a supramolecular gel **1** (1 wt% in toluene). Storage (G′) and loss (G″) moduli recorded during (A) a strain sweep, (B) frequency sweep experiment. (C) Continuous step strain measurements were conducted at 0.1% and 100% strain at 293 K over three repeated cycles, with each cycle monitored for 60 s.

dependence on frequency. This characteristic profile indicates that the gel possesses a predominantly elastic, solid-like nature with a stable three-dimensional network that is resilient to variations in oscillatory frequency. The relatively flat response of G′ and G″ underscores the robustness of the supramolecular architecture, suggesting that the network junctions formed by non-covalent interactions maintain their integrity under dynamic shear conditions. Such behavior is a hallmark of well-developed supramolecular gels, reflecting their potential for applications that require sustained mechanical stability over a broad range of deformation rates.

The thixotropic behavior of supramolecular gel **1** was further examined through continuous step strain measurements at alternating low (0.1%) and high (100%) strain amplitudes over three cycles (Fig. 5C). At each application of high strain (∼60 s, ∼180 s, and ∼300 s), both G′ and G″ display an abrupt decline, with G″ exceeding G′, indicating a transition from an elastic, solid-like state to a viscous, liquid-like state due to the temporary disruption of the supramolecular network under shear. Upon returning to the low strain condition, G′ and G″ progressively recover, with G′ surpassing G″ once more, signifying the restoration of the gel's internal architecture. This reversible shift underscores the gel's thixotropic nature and highlights its intrinsic self-healing ability, where non-covalent interactions such as hydrogen bonding, π–π stacking, and metal–ligand coordination facilitate the reassembly of the network. Such dynamic mechanical responsiveness to

alternating strain not only demonstrates the robustness of supramolecular gel **1** but also points to its potential utility in applications demanding reversible mechanical adaptation, such as injectable soft materials and stimuli-responsive systems.

The viscosity of supramolecular gel **1** was evaluated as a function of shear rate (Fig. 6A). At low shear rates, the organogel exhibits high viscosity, indicating a well-entangled and structured network. As the shear rate increases, the viscosity decreases significantly, suggesting that the supramolecular interactions and entangled fiber structures are progressively disrupted under shear stress. After approximately 100 s^{-1}, the supramolecular gel **1** appears to have fully transitioned into a solution, resulting in an almost constant viscosity value, as shown in Fig. 6A. This shear-thinning behavior is characteristic of non-Newtonian fluids, implying that the material can flow more easily when subjected to an applied force. This property makes it particularly suitable for applications in injectable gels and stimuli-responsive materials.

To observe thixotropic behavior—characterized by reversible viscosity changes under alternating low and high strains—the viscosity of the material was measured under cyclic strain conditions. The results presented in Fig. 6B clearly demonstrate the thixotropic nature of the supramolecular gel. Upon the application of a high strain (100%), the viscosity of the gel markedly decreased, indicative of a disruption in the internal fibrous network under shear. Notably, when the strain was
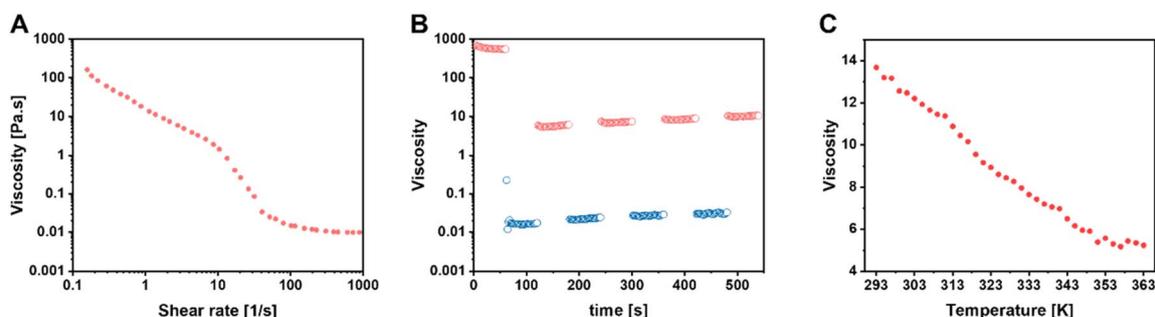

Fig. 6 Viscosity changes of a supramolecular gel **1** (1 wt% in toluene) during (A) shear viscosity as a function of shear rate, (B) continuous step viscosity measurements at 0.1 and 100% and (C) step-wise frequency sweep experiments upon heating from 293 K to 363 K.

subsequently reduced back to a low value (0.1%), the viscosity progressively recovered over time, approaching its original value. This reversible decrease and recovery of viscosity upon alternating strain amplitudes underscore the dynamic, self-healing capabilities of the gel network, characteristic of thixotropic materials. Such behavior highlights the ability of the supramolecular gel to undergo shear-induced structural disassembly followed by spontaneous reformation of the supramolecular architecture, thereby maintaining its mechanical integrity under external stimuli. In addition, the viscosity decreased upon heating (Fig. 6C), indicating the formation of a weak gel structure due to the supramolecular assembly mediated by noncovalent interactions.

Conclusions

We have demonstrated the photophysical and mechanical properties of a supramolecular gel derived from a bisterpyridine ligand. Supramolecular gel **1** exhibits strong blue emission, underscoring its potential for optoelectronic applications. The gel features a distinctive twisted fiber morphology, which was further analyzed through thermodynamic studies. The heating and cooling curves exhibited sigmoidal shapes, indicating that supramolecular gel **1**, prepared in toluene, forms *via* an isodesmic mechanism. The gelator **1** generates fiber structures by a cooperative model with a nucleation and elongation, with a calculated Gibbs free energy of -32.82 kcal mol^{-1} by heating curve. The mechanical properties of supramolecular gel **1** exhibit characteristics typical of non-covalent gel. Notably, the gel demonstrates pronounced thixotropic behavior, indicative of a reversible gelation process. Additionally, supramolecular gel **1** displays tunable viscosity and self-healing properties, making it a promising candidate for advanced material applications, including stimuli-responsive materials and injectable soft matter systems.

Author contributions

J. H. Jung conceptualization, investigation, major experiments, writing original draft, writing – review & editing. Y. Park and M. Nam carried out experimental part; gelation, SEM observation, viscoelastic properties.

Conflicts of interest

There are no conflicts to declare.

Data availability

Additional experimental details as well as the data supporting this article, including materials and methods, ^{1}H NMR, ^{13}C NMR, and FT-IR spectra and thermodynamic parameters, have been included as part of the SI. See DOI: **https://doi.org/10.1039/d5ra03512k**.

Acknowledgements

Notes and references

1 T. Christoff-Tempesta, A. J. Lew and J. H. Ortony, *Gels*, 2018, **4**, 40.

2 H. Wu, J. Zheng, A. L. Kjøniksen, W. Wang, Y. Zhang and J. Ma, *Adv. Mater.*, 2019, **31**, 1806204.

3 A. J. Savyasachi, O. Kotova, S. Shanmugaraju, S. J. Bradberry, G. M. Ó'Máille and T. Gunnlaugsson, *Chem*, 2017, **3**, 764–811.

4 S. Mondal, F. A. Rahimi, T. N. Das, S. Nath and T. K. Maji, *Chem. Sci.*, 2025, **16**, 3646–3654.

5 O. Kotova, R. Daly, C. M. G. dos Santos, M. Boese, P. E. Kruger, J. J. Boland and T. Gunnlaugsson, *Angew. Chem., Int. Ed.*, 2012, **51**, 7208–7212.

6 C. Kim, K. Y. Kim, J. H. Lee, J. Ahn, K. Sakurai, S. S. Lee and J. H. Jung, *ACS Appl. Mater. Interfaces*, 2017, **9**, 3799–3807.

7 G. Yu, X. Yan, C. Han and F. Huang, *Chem. Soc. Rev.*, 2013, **42**, 6697–6722.

8 S. I. Stupp, V. LeBonheur, K. Walker, L. S. Li, K. E. Huggins, M. Keser and A. Amstutz, *Science*, 1997, **276**, 384–389.

9 S. Ganta and D. K. Chand, *Chem.–Asian J.*, 2018, **13**, 3777–3789.

10 J. H. Kim, D. H. Nam, Y. W. Lee, Y. S. Nam and C. B. Park, *Small*, 2013, **10**, 1272–1277.

11 J. H. Park, M. H. Kim, M. L. Seo, J. H. Lee and J. H. Jung, *Polymers*, 2022, **14**, 400.

12 S. Kimura, K. Adachi, Y. Ishii, T. Komiyama, T. Saito, N. Nakayama, M. Yokoya, H. Takaya, S. Yagai, S. Kawai, T. Uchihashi and M. Yamanaka, *Nat. Commun.*, 2025, **16**, 3758.

13 S. Bianco, F. H. Stewart, S. Panja, A. Zyar, E. Bowley, M. Bek, R. Kádár, A. Terry, R. Appio, T. S. Plivelic, M. Maguire, H. Poptani, M. Marcello, R. R. Sonani, E. H. Egelman and D. J. Adams, *Nat. Synth.*, 2024, **3**, 1481–1489.

14 L. Casimiro, F. Volatron, G. Boivin, B. Abécassis, S. Alves, D. Brouri, D. Montero, J. M. Guigner, L. M. Chamoreau, G. Gontard, D. Portehault, Y. Li, A. Proust, R. Lescouëzec, G. Ducouret, A. Solé-Daura, P. Davidson, T. Merland and G. Izzet, *JACS Au*, 2024, **4**, 4948–4956.

15 R. Contreras-Montoya, L. Á. de Cienfuegos, J. A. Gavira and J. W. Steed, *Chem. Soc. Rev.*, 2024, **53**, 10604–10619.

16 J. D. Simpson, L. Thomson, C. M. Woodley, C. M. Wallace, B. Dietrich, A. S. Loch, D. J. Adams and N. G. Berry, *Adv. Mater.*, 2025, **37**, 2415031.

17 P. Sutar and T. K. Maji, *Chem. Commun.*, 2016, **52**, 8055–8074.

18 G. Kuppadakkath, I. Volkova and K. K. Damodaran, *Gels*, 2024, **10**, 584.

19 P. Sutar and T. K. Maji, *Dalton Trans.*, 2020, **49**, 7658–7672.

20 J. Park, K. Y. Kim, S. G. Kang, S. S. Lee, J. H. Lee and J. H. Jung, *Int. J. Mol. Sci.*, 2020, **21**, 4617.

21 S. Panja and D. J. Adams, *Chem. Soc. Rev.*, 2021, **50**, 5165–5200.

22 P. Bertsch, M. Diba, D. J. Mooney and S. C. G. Leeuwenburgh, *Chem. Rev.*, 2023, **123**, 834–873.

23 F. Huang and O. A. Scherman, *Chem. Soc. Rev.*, 2012, **41**, 5879–5880.

24 S. Xu, Z. Zhou, Z. Liu and P. Sharma, *Sci. Adv.*, 2023, **9**, eade3240.

25 R. Zhu, D. Zhu, Z. Zheng and X. Wang, *Nat. Commun.*, 2024, **15**, 1344.

26 N. T. P. Vo, T. U. Nam, M. W. Jeong, J. S. Kim, K. H. Jung, Y. Lee, G. Ma, X. Gu, J. B.-H. Tok, T. I. Lee, Z. Bao and J. Y. Oh, *Nat. Commun.*, 2024, **15**, 3433.

27 X. Huang, R. Li, Z. Duan, F. Xu and H. Li, *Soft Matter*, 2022, **18**, 3828–3844.

28 J. H. Lee, J. Park, J. W. Park, H. J. Ahn, J. Jaworski and J. H. Jung, *Nat. Commun.*, 2015, **6**, 7650.

29 M. Kretschmer, B. Winkeljann, B. A. K. Kriebisch, J. Boekhoven and O. Lieleg, *Commun. Mater.*, 2021, **2**, 97.

30 E. Hui, K. I. Gimeno, G. Guan and S. R. Caliari, *Biomacromolecules*, 2019, **20**, 4126–4134.

31 C. Liang, V. Dudko, O. Khoruzhenko, X. Hong, Z.-P. Lv, I. Tunn, M. Umer, J. V. I. Timonen, M. B. Linder, J. Breu, O. Ikkala and H. Zhang, *Nat. Mater.*, 2025, **24**, 599–606.

32 D. K. Smith, *Soft Matter*, 2024, **20**, 10–70.

33 S. Spagnoli, I. Morfin, M. A. Gonzalez, P. Çarçabal and M. Plazanet, *Langmuir*, 2015, **31**, 2554–2560.

34 J. Bauland, V. Andrieux, F. Pignon, D. Frath, C. Bucher and T. Gibaud, *Soft Matter*, 2024, **20**, 8278–8290.

35 M. Golkaram and K. Loos, *Macromolecules*, 2019, **52**, 9427–9444.

36 E. Vereroudakis, N. A. Burger, L. Bouteiller, B. Loppinet, E. W. Meijer, D. Vlassopoulos and N. J. Van Zee, *Macromolecules*, 2024, **57**, 9030–9040.

37 D. Xu, B. D. Olsen and S. L. Craig, *J. Rheol.*, 2022, **66**, 1193–1201.

38 P. Sutar and T. K. Maji, *Inorg. Chem.*, 2017, **56**, 9417–9425.

39 X. Chen, K. Guo, F. Li, L. Zhou and H. Qiao, *RSC Adv.*, 2014, **4**, 58027–58035.

40 P. Verma, F. A. Rahimi, D. Samanta, A. Kundu, J. Dasgupta and T. K. Maji, *Angew. Chem., Int. Ed.*, 2022, **61**, e202116094.

41 P. Verma, A. Singh, F. A. Rahimi, P. Sarkar, S. Nath, S. K. Pati and T. K. Maji, *Nat. Commun.*, 2021, **12**, 7313.

42 E. G. Lee, H. M. Han, J. H. Jung and S. H. Jung, *New J. Chem.*, 2023, **47**, 22034–22037.

43 G. Picci, C. Caltagirone, A. Garau, V. Lippolis, J. Milia and J. W. Steed, *Coord. Chem. Rev.*, 2023, **492**, 215225.

44 Y. Fang, T. Liu, L. Chen and D. Chao, *ACS Catal.*, 2023, **13**, 2086–2093.

45 E. R. Draper and D. J. Adams, *Chem. Commun.*, 2016, **52**, 8196–8206.

46 G. Zhou, X. Zhang and X. L. Ni, *J. Hazard. Mater.*, 2020, **384**, 121474.

47 A. Sil, A. Maity, D. Giri and S. K. Patra, *Sens. Actuators, B*, 2016, **226**, 403–411.

48 X. Yu, Z. Wang, Y. Li, L. Geng, J. Ren and G. Feng, *Inorg. Chem.*, 2017, **56**, 7512–7518.

49 K. Gandla, K. P. Kumar, P. Rajasulochana, M. S. Charde, R. Rana, L. P. Singh, M. A. Haque, V. Bakshi, F. A. Siddiqui, S. L. Khan and S. Ganguly, *Gels*, 2023, **9**, 121474.

50 M. Kieffer, A. M. Garcia, C. J. E. Haynes, S. Kralj, D. Iglesias, J. R. Nitschke and S. Marchesan, *Angew. Chem., Int. Ed.*, 2019, **131**, 8066–8070.

51 P. Msellem, M. Dekthiarenko, N. Hadj Seyd and G. Vives, *Beilstein J. Org. Chem.*, 2024, **20**, 504–539.

52 M. Weißenfels, J. Gemen and R. Klajn, *Chem*, 2021, **7**, 23–37.

53 Y. Zhang, L. Zhu, J. Tian, L. Zhu, X. Ma, X. He, K. Huang, F. Ren and W. Xu, *Adv. Sci.*, 2021, **8**, 2100216.

54 J. Y. C. Lim, Q. Lin, K. Xue and X. J. Loh, *Mater. Today Adv.*, 2019, **3**, 100021.

55 P. L. Scognamiglio, C. Vicidomini and G. N. Roviello, *Gels*, 2023, **10**, 16.

56 Y. Park, J. Kim and J. H. Jung, *Macromol. Rapid Commun.*, 2025, **46**, 2401004.

57 T. A. Okamura and J. Nakagawa, *Inorg. Chem.*, 2013, **52**, 10812–10824.

58 M. Wehner, M. I. S. Rohr, M. Buhler, V. Stepanenko, W. Wagner and F. Wurthner, *J. Am. Chem. Soc.*, 2019, **141**, 6092–6107.

59 U. Manna, R. Roy, H. K. Datta and P. Dastidar, *Chem.–Asian J.*, 2022, **17**, e202200660.